

The VLT-ASM Seeing and Coherence Monitor

DIMM Upgrade Plan

Document No.: VLT-SPE-ESO-17410-1174
Issue No.: 03.2
Date : August 26, 2003
Prepared by: Marc Sarazin

Change Record

Issue/Rev.	Date	Section/Page affected	Reason/Initiation/Document/Remarks
1.0	17.07.1996		
2.0	19.12.1996	4.	planning updated from Control S/W Func. Spec. Doc. VLT-SPE-ESO-17441-1175 1.0/prep2
		5.1	Added ESO wide current System Diagram
		5.3.2	Corrected encoder /drive data
		5.3.6	Moved Seeing calculation to 6.
		6.	New cosmetic
2.1	24.06.1997		
2.2	23.07.1997	1.2	Table updated
		6.4	Frame Validation Criteria updated
		6.5.1	Variance calculation generalized
2.3	01.08.1998	5.3.5	Mask/prism interface corrected
		6.3	Image Processing Updated
		6.4	S/N calculation generalized
		6.1	Table 3 and Table 5 updated
3.0	01.11.1999	1.2	Table updated
		2.0	Schedule updated
		5.0	removed section on status before upgrade
		7.1.3	added outer scale effects calculation
		7.2	added line of sight extinction calculation
		7.3	added isoplanatic angle calculation
3.1	01.03.2001	1.2	Table.1 updated
		7.2	updated
		7.3	temporarily removed
3.2	06.03.2002	1.2	Table.1 updated
		7.1.3	removed correction of seeing data for large apertures
		7.3	updated isoplanatic angle calculation
		7.4	added coherence time calculation

Contents

1	The VLT Astronomical Site Monitor	5
1.1	ASM General Overview	5
1.2	ASM Major Component List	6
2	Guidelines	8
2.1	DIMM history	8
2.2	DIMM Description	8
2.3	DIMM Upgrade Goal	9
2.4	DIMM Upgrade Schedule	9
3	ASM-DIMM Technical characteristics	9
3.1	Telescope Mount	9
3.2	Telescope Control Electronics	11
3.3	Telescope Control Software	11
3.4	Telescope Optics	12
3.5	Sub-aperture characteristics	13
4	DIMM Functional Description	15
4.1	Parameter Definition	15
4.2	Target Acquisition and Autoguiding	15
5	Image Processing	18
5.1	Photometry	18
5.2	Thresholding	18
5.3	Centroiding	19
5.4	Frame validation	19
6	Statistical Computation	20
6.1	Image Motion	20
6.2	Scintillation	21
6.3	Statistical Validation	22

6.4	Least Square fitting	22
7	Output Parameters	22
7.1	Seeing (DIMM)	22
7.1.1	Seeing Computation	22
7.1.2	Seeing validation	23
7.2	Line of Sight Sky Absorption (LOSSAM)	24
7.2.1	Principle	24
7.2.2	Sequence pre-selection	25
7.2.3	Long exposure photometry	25
7.3	Isoplanatic Angle	27
7.3.1	Theory	27
7.3.2	Scintillation binning	27
7.3.3	Exposure time correction	28
7.3.4	θ_0 computation	29
7.3.5	\bar{h} computation	29
7.3.6	Data output	30
7.4	Coherence Time	31
7.4.1	Direct Measurement	31
7.4.2	τ_0 computation from ASM and meteorological data	31
8	Summary of airmass and wavelength dependency for asm parameters	32

List of Figures

1	Telescope Motion Definition	10
2	Pupil imaging optics	14
3	Atmospheric Extinction and Flux Variability	24
4	Altitude dependency of scintillation aperture weighting functions	28

1 The VLT Astronomical Site Monitor

1.1 ASM General Overview

The Astronomical Site Monitor (ASM) must provide the telescope sub-systems, the telescope operator and the local or remote observer with the appropriate environmental data. It includes a sensing unit composed of a large number of stand-alone sensors, and software units in charge of modeling and prediction tasks and of local data base management.

1. The sensing unit includes all meteorological and atmospheric local sensors with their interfaces to the local control unit for operation and for remote maintenance tasks. A computer communication link with the outside world also allows to collect data from non local sensors delivered by professional meteorological institutes in a machine readable format. Any external information either not in digital format or requiring local meteorological expertise (such as satellite images) is not handled by the ASM. The requirements for the real time output of the unit are enumerated in Table 1.
2. The modeling and prediction unit filters the input flow of information and produces an accurate picture of the current environmental status. In particular, it computes secondary parameters such as water vapour, isoplanatic angle, lifetime, etc...., according to physical models. The predicting unit takes care of the short term predictions of the variables for which local predicting models are available. It also handles the incoming external global forecasts when available. The requirements for the real time output of the unit are enumerated in Table 1.
3. The local data base management unit insures a proper display and logging of information. Display should be interactive and it shall be possible to access ASM data from any VLT user station. ASM data will affect also telescope functions, although it will be up to the VLT Telescope Control Software (VLT-TCS) to decide actions to be performed as a result of changing ASM data. ASM data will have an impact on telescope operations and scheduling, but it is not the purpose of ASM to take initiatives in this sense, except making the new data available with the required reliability. The Local Data Base Management unit also takes care of ASM data storage on removable media.

1.2 ASM Major Component List

Product Structure Item	Current Status	Action Planned	date
17410 <u>Seeing and Sky Monitor</u>			
17411 Tower	OK	Contracted out	1994
17412 Retractable enclosure	OK	Contracted out	1997
17413 Seeing Monitor	OK	in-house upgrade	1997
17413 Coherence Time Monitor	prototype	in-house development	2002
17413 Isoplanatic Angle monitor	prototype	in-house development	2002
17414 Extinction Monitor	OK	in-house development	2001
17414 All Sky (AS) Cloud monitor	none	in-house development	postponed
17415 Infrared Emissivity Monitor	Prototype	cancelled	
17420 <u>Ground Meteorological Station</u>			
17421 Mast	OK	Extend to 30 m	1997
17422 Temperature sensors	OK	Upgrade/Duplicate	1997
17422 Wind Velocity and Direction Sensors	OK	Upgrade/Duplicate	1997
17422 Relative humidity Sensors	OK	Upgrade/Duplicate	1997
17422 Pressure Sensors	OK	Upgrade	1997
17423 Airborne Particle Counter	OK	Purchase	1997
17424 Seismometer	not operational	Purchase	1997
1742X Acoustic Sounder	Prototype at La Silla	Cancelled	
1742Y Atmospheric Profiler	Prototype	Contracted out	2002
17432 Control Electronics Cabin	OK	Purchase	1997

Parameter	Unit	Update interval	Accuracy and/or Resolution
<i>Seeing and Coherence Monitor</i>			
Seeing (DIMM)	arcsec at 500 nm, zenith	1 mn	$\pm 5\%$
Scintillation index	% at 500 nm, zenith	10 mn(*)	$\pm 10\%$
Isoplanatic angle	arcsec at 500 nm, zenith	10 mn(*)	$\pm 20\%$
Coherence Time	ms at 500 nm, zenith	1 mn(*)	20% rms
<i>Satellite Sky Monitor</i>			
Cloud cover	Phot/Variable/Cloudy/Overcast	3 hr(*)	80 % hit, all sky average
Precipitable water vapour	mm H ₂ O	3 hr(*)	1 mm rms, all sky average
<i>Line Of Sight Sky Absorption Monitor</i>			
Rms Relative Flux Variation	percent	10 mn(*)	1
<i>Ground Meteorological Station</i>			
Ground temperature	°C	1 mn	$\pm 0.1^\circ$ C
Air temperature	°C	1 mn	$\pm 0.1^\circ$ C
Relative humidity/dew point	%	1 mn	$\pm 1\%$
Atmospheric pressure	mb	1 mn	$\pm 1\%$
Wind direction	degrees	1 mn	$\pm 5.63^\circ$
Wind velocity	m/s	1 mn	$\pm 2\%$
Airborne particles	particles/m ³	20 mn	$\pm 10\%$
<i>Prediction Unit</i>			
Air temperature	°C	6 hr(*)	1° C rms
Air pressure	mb	6 hr(*)	1 mb rms
Wind velocity	m/s	6 hr(*)	3 m/s rms
Cloud cover	Phot/Variable/Cloudy/Overcast	3 hr(*)	90 % hit, all sky average
Precipitable water vapour	mm H ₂ O	3 hr(*)	1.5 mm rms, all sky average

Table 1: Parameters available from the ASM, (*) currently as web-based operational prototype, (**) currently in development

2 Guidelines

2.1 DIMM history

The Differential Image Motion Monitor (DIMM) is an instrument developed to monitor the turbulence in the atmosphere and its effect on astronomical images.

The parameter measured by the instrument is the seeing, defined as the size (full width at half maximum-FWHM) at $0.5\mu m$, of a one minute exposure image that one would obtain using a large telescope limited by the atmosphere and pointing at zenith.

A prototype system was designed and tested at ESO Garching by M. Cullum and L. Noethe in 1985, the instrument was further developed during the VLT site survey (1986-1990). The first fully automatic version (DIMM2) started routine operation in 1993 at La Silla.

2.2 DIMM Description

The technique employed is based on the statistical analysis of the differential tilt of the wavefront at two locations distant of about 20 cm. The standard deviation of the differential slope of 200 short exposures is converted into the FWHM of a long exposure stellar image by means of appropriate equations ¹

The DIMM was designed to provide the seeing information with an accuracy better than 10%. The accuracy of a properly maintained unit is $\pm 10\%$ at 0.2 arcsec and increases to $\pm 5\%$ for seeing conditions above 1 arcsec.

A prototype coherence monitor mode has been tested in 1992, this option permits to measure the speed at which the wavefront corrugations evolve and to deduct some temporal parameters of the atmosphere ². It requires however short exposures at a few ms intervals which can be obtained using either a fast read-out camera or non-destructive partial frame transfer.

A DIMM has three main components, and some external devices:

- A telescope and its electronics, usually on a tower at five meters above ground to escape from local ground turbulence.
- A CCD detectors and its associated electronics, attached to the telescope by means of adaptors including transfer optics.
- A computer and software, used both for telescope control and data acquisition.
- A link to external devices such as a meteorological station and a retractable enclosure.

¹M. Sarazin, F. Roddier *The E.S.O Differential Image Motion Monitor*; Astron. Astrophys. 227, 294-300 (1990).

²B. Lopez, M. Sarazin; *The ESO atmospheric temporal coherence monitor dedicated to high angular resolution imaging*; Astron. Astrophys. 276, 320-326 (1993).

2.3 DIMM Upgrade Goal

The VLT observatory is equipped with a set of specific monitoring instruments constituting the *VLT Astronomical Site Monitor*. All instruments have to be operated in an automated mode. When not standard from the manufacturer, the instruments should integrate as much as possible VLT standard software and hardware for easier maintenance. The DIMM upgrade will affect all elements of the present configuration, except the telescope itself:

-Software Upgrade: DIMM core SW (automation, sun position, meteo limit conditions, star position, external interrupt handling, data display and storage), high level telescope control (star catalogue, target coordinates, telescope status), low level telescope control (tracking/slewing control, read encoders, motor command) detector control (exposure and centroiding), enclosure control (relays activation), meteo control (serial line handling, clock setting).

-Hardware Upgrade: telescope control electronics (interfaces for encoders, limit switches and motor control), TCCD detectors and associated LCUs, Time reference system, Enclosure control electronics, Serial lines interface.

2.4 DIMM Upgrade Schedule

The upgrade of one monitor (DIMM3, Paranal) should be completed for the VLT integration period. After a test period close to DIMM2 at La Silla, the integration of the DIMM in the VLT-ASM at Paranal was planned in October 1997 (VLT Integration Plan, issue 01). The actual schedule was the following:

April 98: Transportation of DIMM to Paranal, integration of ASM to VLT

February 98: Transportation of DIMM to Paranal, integration of ASM to VLT

July-September 97: Operation at La Silla, Comparison with DIMM2

June 97: Integration and tests of DIMM system at La Silla

Jan-May 97: Integration and Tests Garching

Oct-Dec 96: SW design, HW design

June 96-Sep 96 Analysis ASM software specifications

The La Silla DIMM was then also upgraded as soon as the Paranal system had been accepted: the upgrade took place the first quarter of 1999 with a first light on April 1st, 1999. Data produced by the two DIMMs are available online at:

<http://archive.eso.org/asm/ambient-server>

3 ASM-DIMM Technical characteristics

3.1 Telescope Mount

As Seeing measurements are done preferably close to zenith, an alt-alt mount has been preferred to an altazimutal mount. In such a mount, one fixed rotation axis is along the East/West direction, the second axis is in a vertical plane parallel to the North/South direction as shown on Fig. 1.

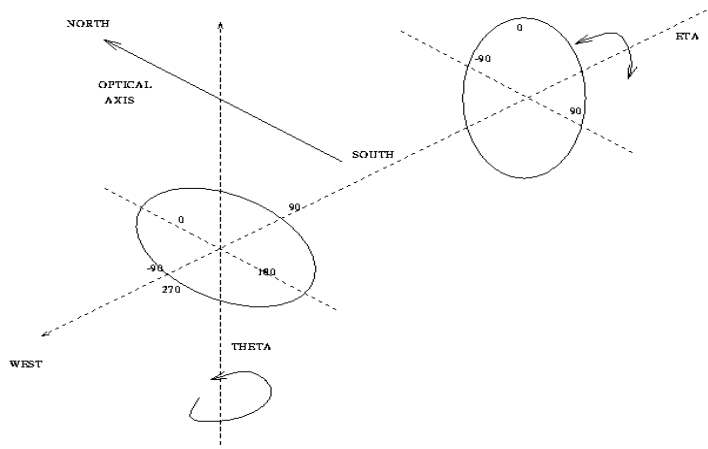


Figure 1: Telescope Motion Definition

- *ETA* Axis

The *ETA* axis is fixed to the foot structure, it is horizontal and oriented East-West. Rotation around the *ETA* axis produces an elevation motion. The zero position is when the optical axis is horizontal. The *ETA* angle varies from 0 to 90 degrees when the telescope points northwards from horizon to zenith; it varies from 0 to -90 degrees when the telescope points southwards from horizon to zenith. It is also called the North-South axis (N/S drive).

- *THETA* Axis

the *THETA* axis is supported by the *ETA* structure and is vertical when *ETA* is 0. Rotation around the *THETA* axis produces an azimuth-like motion. The zero position is when the optical axis points North. The *THETA* angle varies from -90 to +90 degrees when the telescope points northwards from West to East; it varies from +90 to +270 degrees when the telescope points southwards from East to West. It is also called the East-West axis (E/W drive).

- Tracking Zone

The North tracking zone is defined by $-85 < \theta < +85$ and $0 < \eta < 100$.

The South tracking zone is defined by $95 < \theta < +265$ and $-100 < \eta < 0$.

The above limits arise from the following restrictions: the telescope has singular points on the horizon at East and West cardinal points, where the optical axis would be parallel to the *ETA* axis; the telescope can track across the zenith and a little over, but due to mechanical interference between the foot and the focal plane equipment, it must 'flip over' and make a 180 degree rotation around *THETA* when going from the northern half-sky to the southern one and vice-versa. This movement takes several minutes, for that reason also the star catalogue used in seeing monitor mode is limited to objects in the southern half-sky.

- Special positions

North sleeping position: the optical axis is horizontal and points to the North ($\eta = 0$, $\theta = 0$ degrees).

South sleeping position: the optical axis is horizontal and points to the South ($\eta = 0$, $\theta = 180$ degrees).

Dismount Position: starting from the North sleeping position, the optical axis is flipped 90 degrees to point vertically.

- Status Flags

When the telescope current position (η , θ) is displayed, six status digits are also provided. They have the following meanings, from left to right:

'1' = manual paddle mode enabled

'1' = telescope is tracking

'0' = *ETA* positive limit switch activated

'0' = *ETA* negative limit switch activated

'0' = *THETA* positive limit switch activated

'0' = *THETA* negative limit switch activated

3.2 Telescope Control Electronics

- Gear: the telescope is linked to each motor by a 2 stage harmonic drive reduction gear with a factor of 80x260:1.
- Encoders: two encoders per AXEM 12M2 motor, a slow encoder directly on the output shaft gives a theoretical pointing resolution of $90 \times 3600 / 4096 = 79$ arcsec. The fast encoder benefits from a 260x2:1 reduction of an harmonic drive (0.152 arcsec tracking resolution).
- Joystick: the joystick is to be used only for troubleshooting procedures. Its action is completely independent from the processor hardware and software. When the joystick is connected, the power amplifiers inputs are decoupled from the motor control cards and connected to the joystick's potentiometers.
- Hand Paddle: the hand paddle replaces the joystick for manual slewing and tracking correction under processor hardware and software control.
- A tilt switch is located inside the focal plane equipment, its purpose is to disconnect power from the drives if the telescope secondary goes below the horizontal plane due to some malfunction. Its status is however not reported by the control software. The device is based on an inductive proximity switch normally carrying a steel ball.

3.3 Telescope Control Software

The time between successive messages sent to the telescope control electronics via the serial line must not be smaller than 0.1 s. The telescope has three normal states: idle, slewing and tracking.

- Target Star Identification: a resident star catalogue is read. The brightest star with negative hour angle is chosen.
- Telescope Tracking Initiation: the target start coordinates (Hour Angle, Right Ascension) are converted into telescope position angle (θ , η). These are sent to the telescope control electronics along with the tracking duration above which the telescope tracking is automatically halted. The telescope starts tracking when the position is reached.
- Telescope Position Query: the telescope processor returns the motor positions θ and η in degree with one significative digit.

- Telescope Position Control: software limits are preset to prevent the telescope to reach hardware limit positions. They are defined as:
 - the horizon
 - the big circle East-Zenith-West (tolerated overshoot $Z = 10$ degree)
 - the singular points of East and West horizon (safety margin $L = 5$ degree)
 When the telescope reaches the software limits listed in Table 2, a Telescope Tracking Termination command must be sent to the control electronics.
- Telescope Autoguiding Loop: feedback from the CCD control software is forwarded to the telescope control electronics as θ and η offsets in units of $1/300$ arcsec. Such commands are accepted in tracking state only.
- Target Star Position control: the tracking is halted and a new target is chosen when the star hour angle exceeds $+3$ hours.
- Telescope Tracking Termination: tracking is stopped, the telescope returns to idle state.
- Telescope Slewing Initiation: send the telescope to a given position (within the software limits). The telescope stops and returns to idle state when the position is reached.
- I/O Management: commands relay status for enclosure control, reads analog inputs, sets analog outputs.

Telescope	Pointing North	Pointing South
big circle	$\eta > 90 + Z$	$\eta < -90 - Z$
horizon	$\eta < 0$	$\eta > 0$
East singular point	$\theta > 90 - L$	$\theta < 90 + L$
West singular point	$\theta < -90 + L$	$\theta > 270 - L$

Table 2: Telescope Control Software Limits.

3.4 Telescope Optics

Because of requirements on the size and distance of the sub-apertures, the minimum diameter of the telescope free aperture is 240 mm.

For the first tests in February 86, the instrument was attached to a 11" Celestron telescope. In August of the same year, a 350 mm Cassegrain on an Alt-Alt mount was delivered, developed in Belgium by AMOS S.A. especially for this purpose. ESO now owns three such telescopes with the following optical characteristics:

1. Telescope
 - Cassegrain telescope
 - Primary mirror: parabola, clear aperture 350 mm, $F/2$.
 - Secondary mirror : hyperbola
 - F /ratio at cassegrain focus: $F/15$.
 - Back focal distance measured from vertex of M1: 100.0 ± 0.1 mm.
 - Distance between vertices of M1 and M2: 605.9 ± 1 mm.
 - Field of view: ± 5 arcmin (± 7.9 mm).

2. Mirror 1: Parabola, lightened
 - Overall maximum diameter: 380 mm, to be defined by supplier to meet specifications on the clear aperture optical quality.
 - F/ratio: F/2 with a clear aperture of 350 mm diameter.
 - Material: zerodur
 - Mirror thickness at center: 50 mm
 - Central hole diameter: 55 mm \pm 0.2
 - Center hole edges beveling: maximum 2 mm on optical surface
 - Support: the mirror will be supported by its center part.
 - Minimum weight reduction: 25 % from full cylinder, by proper machining of the back surface, either spherical or conical
 - Minimum diameter of backplate flat central part:70 mm

3. Mirror 2: Hyperbola
 - Clear aperture: 50 mm.
 - Overall maximum diameter: 57 mm.
 - Radius of curvature: -217.2 mm.
 - Exentricity: -1.71
 - Material: zerodur.
 - Thickness: 12 mm.

4. Optical quality:

The image quality of the final cassegrain combination must correspond to 80 % of energy concentrated in less than 24 μ m on axis and 35 μ m off axis (5arcmin.) at 5000 Å.

If double pass interferometry is used for acceptance tests, maximum allowable wavefront distortions for the telescope are $\lambda/4$ for low frequencies (astigmatism, spherical aberrations), and $\lambda/10$ rms for high frequencies.

5. Coating:

Mirror 1 and 2 are aluminized and protected for use in the visible.

3.5 Sub-aperture characteristics

For more commodity in changing pupils characteristics, the entrance pupil of the telescope of diameter Φ and F/ratio F_r is re-imaged behind the Cassegrain focus with a collimator as shown on Fig. 2. This also permits to install the DIMM at the focus of any telescope with only minor changes.

In the telescope pupil image plane, a roof prism of angle A is used to shift symmetrically the star images as viewed through two subapertures in the direction parallel to their separation axis. To create subapertures of diameter D and separation d , the plane edge of the prism is covered by a pupil mask consisting of two holes of diameter γD and distant of γd . γ is the magnification of the optical system given by:

$$\gamma = \frac{f}{F_r \Phi} \quad (1)$$

where $F_r \Phi$ is the telescope focal length (F/ratio times diameter) and f is the collimator focal length. The axial position of the mask coincides accurately with the conjugate image of the primary mirror of the telescope which is usually considered as the entrance pupil.

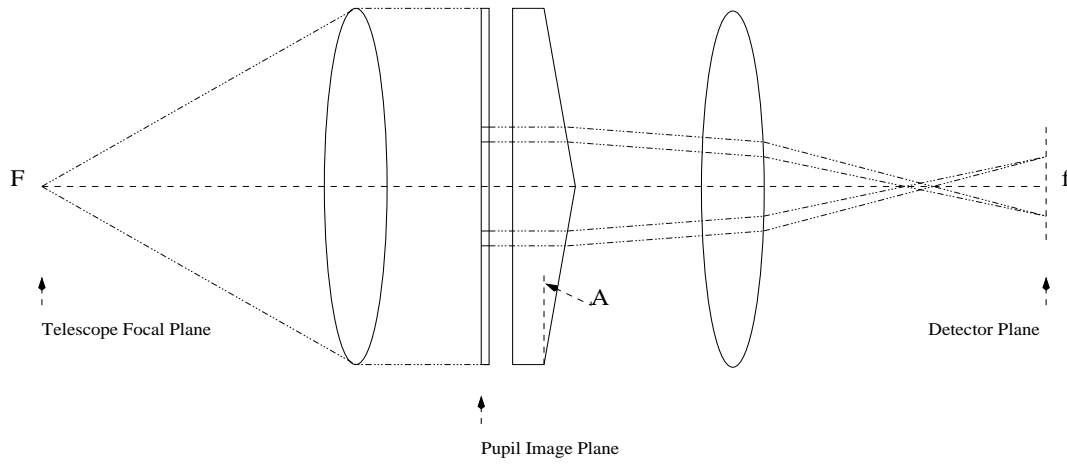


Figure 2: Optical pupil imaging system for subaperture creation

The star image displacement of each image in the detector plane due to a prism of angle A (in degree) is then, for small angles:

$$L = f(n_{prism} - n_{air}) \tan A \quad (2)$$

The prism and mask physical characteristics should remain within specification in the whole operational temperature range. Chromatic displacement in the detector plane shall be smaller than 100 nm in the visible range.

The light beams should not hit the roof edge in the whole field of view defined by the detector largest dimension (eg. using a 400x290 CCD with 22 μm pixels, the maximum incidence angle on the prism is 6 degree, thus a shift of the beams at the roof edge by ca. 1.8 mm after crossing the 12 mm thick plate. This margin is to be taken into account to determine the maximum hole diameter for a given hole separation. In this calculation, the roof edge is supposed infinitely thin.

- Roof Prism

Material: Silica (index $n_{prism} = 1.458$ in the visible)

Diameter: 25 mm $+0/-0.1$

Thickness: 9 mm ± 0.1

Angle $A = 1.5$ degree ± 30 arcsec, constant within ± 1 arcsec

Surface quality: better than $\lambda/4$ (V) up to within 0.1 mm distance from the edge.

Coating: anti-reflection on the flat face

- Mask

Material: Bronze Beryllium, both sides non reflecting in the visible, Circular shape

Diameter: 15 mm

Thickness 0.2 mm

Holes: two circular holes, diameter 0.9 mm ± 0.02 , distance 1.5 mm ± 0.02 , centered on the mask center.

- Mechanical Assembly Procedure

-cement mask into prism holder: orientation of the holes axis better than 1 degree

-cement prism into prism holder: orientation of the prism roof edge (perpendicular to the hole

axis) better than 10 arcmin

-dimensional control: exact final configuration is measured and a report is included in furniture

The part will be used in open air without direct sunshine under temperature ranging from -10 Celcius to 30 Celcius annually. Temperature gradient during operation does not exceed 2 Celcius per hour. Relative humidity can vary from 0% to 80%, no condensation.

4 DIMM Functional Description

4.1 Parameter Definition

The parameters entering the calculation of seeing are divided in three categories. The setup parameters (Table 3) are constants mainly dependent on hardware. The exposure parameters (Table 4) are computed at each individual exposure. It is reminded that a CCD frame may contain several exposures as in the coherence monitor mode. The sequence parameters (Table 5) are obtained after the required number of exposures have been processed, they are used for the final computation of the output parameters (Table 6).

4.2 Target Acquisition and Autoguiding

It is assumed that the telescope presetting is accurate enough to bring the target in the field of view of the detector. A full CCD frame is read-out, thresholded in the standard way (twice the average illumination) and the cdg of the remaining pixels defines the target coordinates. Tracking corrections are necessary to center the target to the requested operating position ($X d_0, Y d_0$ or $X c_0, Y c_0$ according to the operating mode) before starting the measurements. The centering accuracy should be better than ± 5 arcsec so as to bring a star image inside each of the two preset subarray position.

It is assumed that the telescope tracking is accurate enough to maintain the target within ± 30 arcsec of the operating position for the duration of one measurement sequence (typically one minute). New tracking corrections are made if necessary at the beginning of each sequence, based on the average centroid of the last 10 frames of the previous sequence (to average out wind effects).

Parameter	Variable	Default Value	Unit
1 arcsec	ρ	$\frac{\pi}{180.3600} = 4.84 \text{ E-}06$	radian
Telescope Diameter	Φ	.35	m
Telescope F ratio	F_r	15	
Objective Focal Length	f	.040	m
Pupil Mask Prism Angle	A_h	1	degree
Mask Hole Diameter	D_h	.0009	m
Mask Hole Separation	d_h	.0015	m
Pupils Diameter	$D = D_h \frac{F_r \Phi}{f}$.118	m
Pupils Separation	$d = d_h \frac{F_r \Phi}{f}$.200	m
CCD size (X,Y)	CCD _x , CCD _y	386x290	pixel
CCD noise floor	a_f	$3\sigma(a_0)$	A/D Count
CCD Subarray size	n, n	20x20	pixel
Pixel size (X,Y)	P_x, P_y	22x22 E-06	m
Pixel Angular Pitch (nominal)	$p0_x, p0_y = \frac{1}{\rho} \left(\frac{P_x, P_y}{F_r \Phi} \right)$	0.84x0.84	arcsec
Pixel Angular Pitch (measured)	p_x, p_y	0.81x0.81	arcsec
Spot Axis Rotation (vs CCD x axis)	α_0	0	radian
Spots Separation (nominal)	$W_0 = \frac{f \tan A_h / 2}{P_x}$	32	pixel
Nbr of Frames per Sequence	N_0	800	
Wavelength (FWHM)	λ	0.5E-6	m
Star Coordinate	α, δ		hour, degree
Star Magnitude	M		V band
<u>DIMM MODE:</u>			
Exposure Time	T_d	53E-04 ± 1 %	s
Nbr of Exposures per frame	N_c	1	
Autoguiding Target (X,Y)	$Xd_0, Yd_0 = \frac{\text{CCD}_x}{2}, \frac{\text{CCD}_y}{2}$		pixel
<u>SKY MONITOR MODE:</u>			
Equivalent Long Exposure	T_l	600	s
Min Image Background	sbg_{min}	50	ADU
Max rms Background	$rmsbg_{max}$	1	ADU
Max short Exposure Deviation	$maxdT_d$	1E-04	s
Min Number of Sequences	N_{lmin}	5	
Photometric Sky Limit	RF_{lrms}^{max}	0.016	
Max Flux Imbalance	DRF_{max}	0.1	
Max Scint Imbalance	DRS_{max}	0.35	
<u>COHERENCE MODE:</u>			
Exposure Time (Coherence Mode)	T_c	1E-03 ± 10 %	s
Nbr of Exposures per frame	$N_c = \frac{\text{CCD}_y}{n}$	14	
Autoguiding Target (X,Y)	$Xc_0, Yc_0 = \frac{\text{CCD}_x}{2}, \frac{\text{CCD}_y}{2} - n \frac{N_c}{2}$		pixel
<u>VALIDATION:</u>			
Threshold for centroiding	k_t	9	rms of background
Nbr. Centroiding non-zero	n'_{min}	3	Pixel
Saturation Limit	k_r	0.9	Max(A/D Count)
S/N Ratio Limit	S/N _{min}	5	
Rejected Exposure limit	k_n	75	% of N_0
Spot Elongation Limit	k_e	10	%
Spot Decentering Limit	k_f	2	Spot fwhm
Gaussian Clipping Limit	k_c	3	rms of distribution
Instrumental noise	$\frac{\sigma_{n\parallel}^2}{(p_x \rho)^2}, \frac{\sigma_{n\perp}^2}{(p_y \rho)^2}$	0.01 ± 0.002	pixel ²
Statistical Error Limit	k_s	1	

Table 3: DIMM Upgrade Setup Parameters. (X,Y) coordinates are along CCD lines and columns, Pixel (1,1) is in the upper left corner.

Parameter	Variable	Unit
Spot1 cdg	x_1, y_1	pixel
Spot2 cdg	x_2, y_2	pixel
Image cdg (for subarray tracking)	$x_g, y_g = \frac{1}{2}(x_1 + x_2), \frac{1}{2}(y_1 + y_2)$	pixel
Spot1 Flux	A_1	A/D count
Spot2 Flux	A_2	A/D count
Spot1 fwhm	f_{x1}, f_{y1}	pixel
Spot2 fwhm	f_{x2}, f_{y2}	pixel
Nbr illuminated	n'	pixel

Table 4: DIMM Exposure Parameters

Parameter	Variable	Unit
Airmass	$(\cos\gamma)^{-1}$	
Image cdg (for autoguiding)	\bar{X}_g, \bar{Y}_g	pixel
Spot Separation (measured)	W_g	pixel
Spot Axis Rotation (vs CCDX)	α_g	radian
Actual Exposure Time	T_d	ms, average and rms
Signal/Noise Ratio	S/N	average
Validated Exposures	N'	total
Rejected Exposures		total/clipping only
Spot1 Flux	F_1	A/D count
Spot2 Flux	F_2	A/D count
Spot1 Scintillation Index	S_1	percent
Spot2 Scintillation Index	S_2	percent
Seeing parallel	FWHM_{\parallel}	arcsec
Seeing perpendicular	FWHM_{\perp}	arcsec
Nbr validated	N'	exposures

Table 5: DIMM Sequence Parameters (internal history data)

Parameter	Variable	Unit
Airmass	$(\cos\gamma)^{-1}$	
Wavelength	λ	m
Seeing	FWHM	arcsec
Line of Sight	α, δ	hour, degree
Rel. Flux Variation	RF_{rms}	ratio
Isoplanatic Angle	θ_0	arcsec

Table 6: DIMM Output Parameters (public data)

5 Image Processing

5.1 Photometry

The basic algorithm for centroid determination uses the algebraic definition of the center of gravity without any gaussian fitting process.

The sub-arrays are treated as matrices $[A] = [a_{i,j}]$ where $a_{i,j}$ is the pixel A/D count and i, j its coordinates in the frame of the sub-array.

A saturation test is performed, checking that $\text{MAX}[A] \leq k_r \text{MAX}(A/D \text{ count})$. Should the image be recursively saturated, the exposure time would have to be shortened.

Before any centroid computation, but after the saturation tests, the average bias + sky background is subtracted from the images.³

Let the matrix $[A0] = [a0_{i,j}]$ be a sub-array of dimension $n_0 \times m_0$ taken at an empty section of the frame. The average sky background per pixel is:

$$\bar{a}_0 = \frac{1}{n_0 m_0} \sum_{i=1}^{n_0} \sum_{j=1}^{m_0} a0_{i,j} \quad (3)$$

In practice, as images contain one single bright object, the background is calculated from the average of the three least illuminated corners, with $n_0 = m_0 = \frac{n}{4}$. The sky background is more accurately obtained with the analysis of the histogram of the flux distribution among the pixels: the position and width of the highest peak determine \bar{a}_0 and It is possible to compute A , the total illumination in the sub-array

$$A = \sum_{i=1}^n \sum_{j=1}^n (a_{i,j} - \bar{a}_0) \quad (4)$$

5.2 Thresholding

Images taken with short exposure times through small apertures show important flux variations due to stellar scintillation. The pixels used for centroid determination are selected by comparison to a minimum flux value. This threshold should be proportional to $\sigma(a_0)$, the rms of the background. The coefficient of proportionality k_t is hardware dependent (see ASM Commissioning Reports for actual values).⁴ All pixels below the threshold $k_t \sigma(a_0)$ are set to zero and n' is the total number of remaining non-zero pixels ($n' \leq n^2$)

For each spot centroid determination, the number n' of non-zero pixels should not be less than a preset limit n'_{min} determined by the algorithm chosen. In addition the non-zero pixels should be adjacent.

³For short exposures with negligible sky background taken with a frame transfer cooled CCD with electronic shuttering, a fixed reference frame (bias) provided with the chip could be used in place of dark subtraction. However this was not applicable because the camera we used had an open pelletier control loop. The bias level was thus variable depending on the cooling temperature, itself linked to the outside air temperature. For further photometry processing (scintillation and extinction), sky background variations are not negligible, in particular with the moon in the vicinity of the field of view

⁴However, when using a low read-out noise camera and when the limiting magnitude requirements are not stringent, this factor can be replaced by an arbitrarily defined constant floor level a_f

This latter requirement (connexity of the non-zero pixels) is lifted in the case of speckle images analysis as happens in the coherence mode of the DIMM (1 ms exposures).

5.3 Centroiding

The matrices are then summed in columns and rows, giving the vectors :

$$\mathbf{A}_x = [A_i] \quad \text{with } A_i = \sum_{j=1}^n a_{i,j} \quad (5)$$

$$\mathbf{A}_y = [A_j] \quad \text{with } A_j = \sum_{i=1}^n a_{i,j} \quad (6)$$

The coordinates of the center of gravity of the remaining illumination inside the subarrays are then:

$$x_s = \frac{1}{\sum_{i=1}^n A_i} (\mathbf{A}_x \cdot \mathbf{X}) = \frac{\sum_{i=1}^n A_i i}{\sum_{i=1}^n A_i} \quad \text{with } X_i = i \quad (7)$$

$$y_s = \frac{1}{\sum_{j=1}^n A_j} (\mathbf{A}_y \cdot \mathbf{Y}) = \frac{\sum_{j=1}^n A_j j}{\sum_{j=1}^n A_j} \quad \text{with } Y_j = j \quad (8)$$

5.4 Frame validation

Any measurement rejection should generate a log message with the time, reason and numerical value of the parameter involved. Infinite loops should be prevented by means of error counters and limits above which the measurement procedure would be re-initialized (eg. choosing another star).

To check optical quality and detect possible vignetting, the FWHM of each spot is estimated in both directions yielding (f_{x_s}, f_{y_s}) , using a standard focus sequence algorithm. The elongation of an image, defined as the ratio $\frac{f_{x_s}}{f_{y_s}}$ should not be more than $\pm k_e\%$ from unity or the data is discarded and the loop is resumed with an updated subarray position.

Each spot is checked for the centering inside its subarray. Should one of the points be found too close to a side of its subarray

$$\text{MIN}(x_s, n - x_s) \leq k_f f_{x_s} \text{ or } \text{MIN}(y_s, n - y_s) \leq k_f f_{y_s} \quad (9)$$

the data is discarded and the loop is resumed with an updated subarray position.

The S/N ratio of each spot is checked independently because scintillation effects are not correlated: the S/N ratio is defined as the ratio of the total illumination in the object after background subtraction to the total background noise in the pixels above threshold (see Doc. VLT-TRE-ESO-17240-1689).

$$\text{S/N} = \frac{A}{n' \sigma(a_0)} \quad (10)$$

This definition has however the inconvenient to make the S/N dependent on the minimum threshold which is also a user configurable parameter. ⁵

A frame with one of the spots at $\text{S/N} \leq \text{S/N}_{\min}$ is discarded and the loop is resumed with an updated subarray position.

⁵A more useful parameter for the DIMM working sometimes in the vicinity of the full moon would be the signal to background ratio. The S/B ratio is defined as the ratio of the average illumination from the object (average flux per usefull pixel after background subtraction) to the average background in the stellar image. The stellar image area is

After the validation test, the relevant exposure parameters (Table 4) are computed: combining the spots coordinates in their subarrays with the absolute position of each subarray in the CCD, one obtains then two couples of coordinates of center of gravity (x_1, y_1) and (x_2, y_2) . The current centerfield position is computed along:

$$x_g, y_g = \frac{1}{2}(x_1 + x_2), \frac{1}{2}(y_1 + y_2) \quad (12)$$

(x_g, y_g) determines the next subarray positions to take into account tracking errors. However the measurements of several previous frames should be used as indicated in 4.2. This filtering is recommended for wind shake rejection.

The two illumination values A_1 and A_2 are stacked for later composing an equivalent long exposure F to be processed in the Line of Sight Sky monitor as indicated in §7.2.

Out of N_0 frames requested, N have passed the frame validation tests. The sequence shall be accepted if $N_0 - N < k_n N_0/100$

6 Statistical Computation

6.1 Image Motion

After the number N_0 of exposures for the sequence is reached the following statistical parameters are computed using the data from the N validated exposures:

-the coordinate of the image cdg for autoguiding

$$\bar{X}_g = \frac{1}{2N} \sum_{j=1}^N (x_1(j) + x_2(j)) \quad (13)$$

$$\bar{Y}_g = \frac{1}{2N} \sum_{j=1}^N (y_1(j) + y_2(j)) ; pixel \quad (14)$$

-the average separations of the spots in each axes

$$\bar{d}_{xg} = \frac{p_x \rho}{N} \sum_{j=1}^N (x_1(j) - x_2(j)) \quad (15)$$

$$\bar{d}_{yg} = \frac{p_y \rho}{N} \sum_{j=1}^N (y_1(j) - y_2(j)) ; radian \quad (16)$$

calculated from the Full Width at Half Maximum fits (see Doc. VLT-TRE-ESO-17240-1689):

$$S/B = \frac{A}{4f_{x_s} f_{y_s} \bar{a}_0} , \quad (11)$$

this assumes that the background is constant over the image, ie. the residual image background has a zero average after sky background subtraction, and thus does not enter in the total illumination A of the object. Also this works only when bias subtraction is performed first, so that the background measured on the image corners is produced only by the sky (moon, clouds illuminated by the moon). It is not applicable in the case of the ASM (no bias subtraction because of thermal drifts).

-the average separation W_g and the rotation α_g with respect to the CCD line axis (α_g should be close to 0 with the VLT TCCDs).

$$W_g = \sqrt{\bar{d}_{xg}^2 + \bar{d}_{yg}^2} \quad (17)$$

$$\alpha_g = \arctan \frac{\bar{d}_{yg}}{\bar{d}_{xg}} \quad (18)$$

-the variance of the differential motion is computed over directions parallel and perpendicular to the spot separation axis:

$$\sigma_{g\parallel}^2 = \frac{1}{N} \sum_{j=1}^N \left[dpara_g(j) - \frac{1}{N} \sum_{i=1}^N dpara_g(i) \right]^2 \quad (19)$$

$$\sigma_{g\perp}^2 = \frac{1}{N} \sum_{j=1}^N \left[dperp_g(j) - \frac{1}{N} \sum_{i=1}^N dperp_g(i) \right]^2 ; \text{radian}^2 \quad (20)$$

with

$$dpara_g(j) = (x_1(j) - x_2(j))p_x\rho \cos \alpha_g + (y_1(j) - y_2(j))p_y\rho \sin \alpha_g \quad (21)$$

$$dperp_g(j) = -(x_1(j) - x_2(j))p_x\rho \sin \alpha_g + (y_1(j) - y_2(j))p_y\rho \cos \alpha_g \quad (22)$$

6.2 Scintillation

The average flux of an equivalent long exposure of duration NT_d is computed for each spot:

$$F_1 = \frac{1}{N} \sum_{j=1}^N A_1(j) \quad (23)$$

$$F_2 = \frac{1}{N} \sum_{j=1}^N A_2(j) ; \text{A/Dcount} \quad (24)$$

and then the scintillation index defined as the ratio of the variance of intensity fluctuations to the square of the average flux:

$$S_1 = \frac{1}{F_1^2} \frac{1}{N} \sum_{j=1}^N (A_1(j) - F_1)^2 \quad (25)$$

$$S_2 = \frac{1}{F_2^2} \frac{1}{N} \sum_{j=1}^N (A_2(j) - F_2)^2 \quad (26)$$

$$(27)$$

It is not foreseen to deliver the scintillation index as public data in the DIMM mode because the measurement bandwidth is smaller than the atmospheric scintillation temporal fluctuations. It is however a useful engineering tool for controlling the instrumental status.

6.3 Statistical Validation

The theory assumes that the image motion is a gaussian variable. It can happen that turbulence close to ground level shows sporadic small scale discrepancies. This is monitored by clipping the differential motion data set within $\pm k_c$ times the rms of the distribution. The final variance is then re-calculated over the clipped data sets (of size $N' \leq N$). The number $N - N'$ of rejected exposures should not be more than a few percent k_c of the total, it is moreover a useful engineering tool for controlling the instrumental status.

6.4 Least Square fitting

An additional check has been introduced for the detection of a particular instrumental noise source due to unwanted variations of the relative spot position within the course of the sequence. The time series of differential position along the CCD axes ($x_1 - x_2$ and $y_1 - y_2$) are checked for any non zero mean trend which is then fitted and removed. A well designed system should show virtually no difference between unfitted and fitted data.

7 Output Parameters

7.1 Seeing (DIMM)

7.1.1 Seeing Computation

For a given wavefront of coherence radius r_0 the variance of the differential motion between two pupils of diameter D at the distance d of each other depends on the direction of measurement:

$$\sigma_{\parallel}^2 \simeq 2\left(\frac{3.44}{2\pi^2}D^{-1/3} - 0.097d^{-1/3}\right)\lambda^2 r_0^{-5/3} \quad (28)$$

$$\sigma_{\perp}^2 \simeq 2\left(\frac{3.44}{2\pi^2}D^{-1/3} - 0.145d^{-1/3}\right)\lambda^2 r_0^{-5/3} ; \text{radian}^2 \quad (29)$$

We note that direction dependent sensitivity of the image motion to changes in seeing quality is given by the constant coefficients:

$$K_{\parallel} = 2\left(\frac{3.44}{2\pi^2}D^{-1/3} - 0.097d^{-1/3}\right)$$

$$K_{\perp} = 2\left(\frac{3.44}{2\pi^2}D^{-1/3} - 0.145d^{-1/3}\right)$$

Finally the site quality defined as the long exposure FWHM at the wavelength λ and at zenith is related to the variance of the image motion measured in either direction $*$ at zenith angle γ by:

$$\text{FWHM}_* = \frac{1}{\rho} 0.976\lambda/r_0 = \frac{1}{4.9710^{-6}}\lambda^{-1/5} \left[\frac{(\sigma_{g*}^2 - \sigma_{n*}^2) \cos \gamma}{K_*} \right]^{3/5} ; \text{arcsec} \quad (30)$$

where σ_{n*}^2 is the additive instrumental noise (in radian squared) initially measured in the laboratory on simulated fixed spots, and ρ is the arcsec to radian conversion factor (Table 3).

7.1.2 Seeing validation

The two FWHMs obtained after subtraction of the instrumental noise should be equal within the statistical error on the variance computed with a finite number N' of samples:

$$\frac{\Delta(\sigma_*^2)}{\sigma_*^2} = \sqrt{\frac{2}{N' - 1}} \quad (31)$$

a validation factor k_s is introduced and the measurement rejected (ie: no public output) when:

$$\frac{2 | \text{FWHM}_{\parallel} - \text{FWHM}_{\perp} |}{\text{FWHM}_{\parallel} + \text{FWHM}_{\perp}} > 2k_s \frac{3}{5} \sqrt{\frac{2}{N' - 1}} \quad (32)$$

The final result is the average of both at $\lambda = 0.5 \mu\text{m}$ expressed in arcsec:

$$\text{FWHM} = \frac{1}{2}(\text{FWHM}_{\parallel} + \text{FWHM}_{\perp}) \quad (33)$$

Along with the FWHM the reference time at end of sequence (N^{th} exposure), the corresponding time span dt between the first and the last exposure of the sequence has to be indicated so that time series of long duration (typ. longer than a few minutes) are rejected.

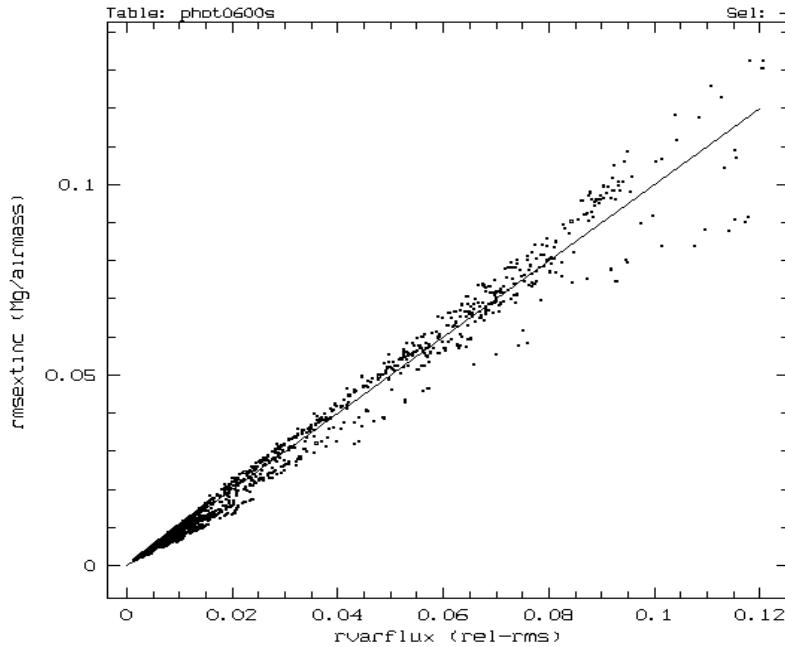


Figure 3: Comparison of rms atmospheric extinction variations and rms flux variation over 10mn exposures

7.2 Line of Sight Sky Absorption (LOSSAM)

7.2.1 Principle

The main purpose of this mode is to detect non photometric sky by measuring the variation of the stellar flux along the line of sight of the DIMM. The extinction E is obtained by comparison of the actual flux to the DIMM star catalogue reference value $\log(F_0)$ after correcting for airmass.

$$E = -2.5 \frac{\log(F) - \log(F_0)}{\cos \gamma^{-1}} ; \text{Magnitude} \quad (34)$$

It was initially planned to directly monitor the atmospheric extinction but this was not possible due to the long term unstability of the detector (temperature drifts) and the lack of control on the instrumental constant (the telescope is a maintenance free automated device). It was however demonstrated (and generally accepted in the community) that the variability of the extinction coefficient over limited time scales can be approached by measuring directly the variability of the flux itself.

Fig. 3 shows the correlation between the relative rms flux variation and the rms of the extinction coefficient for the month of June 2000 at La Silla. The extinction coefficient is determined by aperture photometry relative to an arbitrary reference corresponding for each star to the best conditions of the month. Setting the photometric sky limit at 0.015, the use of rms flux variations induces a discrepancy (false alarm) on the determination of non photometric sky less than 7% of the time with a 10% margin, and only 2% of the time with a 20% margin.

The flux variability is estimated over an equivalent long exposure reconstructed from several DIMM sequences taken on the same star. All the constants used in this section are defined in Table 3 (Sky Monitor Mode).

At the end of each DIMM sequence, the sky subtracted fluxes on both apertures, F_1 and F_2 , in counts per unit of time, are calculated from the N' valid short exposures of duration T_d (equ. 24). The average flux is then:

$$F_d = \frac{1}{2}(F_1 + F_2) \quad (35)$$

For our purpose, the noise due to clear sky scintillation has to be averaged out by building an equivalent long exposure over a longer time T_l . This involves the N_l DIMM sequences which took place in the last T_l seconds on the same star. Note that N_l changes with observing conditions (eg high wind reduces the DIMM data output rate).

7.2.2 Sequence pre-selection

Before it can be included into a long exposure equivalent, the photometric reliability of each sequence is tested.

The mean actual exposure time T_{dact} is a parameter produced by the TCCD image processing software at the end of each DIMM sequence. It has been noted that a departure from the preset value was generally associated to corrupted photometric data. We define a maximum error margin $maxdT_d$ and perform the test:

$$|T_{dact} - T_d| \leq maxdT_d \quad (36)$$

The sub image backgrounds $Sbg_{1,2}$ and the rms variation $rmsbg$ are parameters produced by the TCCD image processing software at the end of each DIMM sequence. In presence of straylight contamination due to direct moonlight or to moonlit cloudy sky, the sky absorption cannot be computed with enough accuracy. For that purpose, tests are made on the image background characteristics. First, it has been noted that unusually low background values were generally associated to corrupted photometric data:

$$Sbg_1 > Sbg_{min} \quad (37)$$

$$Sbg_2 > Sbg_{min} \quad (38)$$

secondly check the background temporal stability

$$rmsbg < rmsbg_{max} \quad (39)$$

and then compute the average background for the sequence

$$Sbg_d = \frac{1}{2}(Sbg_1 + Sbg_2) \quad (40)$$

7.2.3 Long exposure photometry

It is necessary to combine a number N_l of selected sequences for building a long exposure average so that it corresponds to a total shutter open time T_s . N_l should be larger than N_{lmin} , chosen large enough so that the statistics is meaningful. The long exposure is constructed by moving backward in time and adding to the current sequence all the sequences of the previous T_l seconds on the same star. The equivalent shutter open time of the N_l sequences so assembled is

$$T_s = \sum_{j=1}^{N_l} N(j)T_{dact}(j) \quad (41)$$

where $N(j)$ is the number of validated short exposures used to compute the sequence photometric parameters sequence (j). Note that a minimum shutter open time is implicitly set because a lower limit was imposed on $N(j)$ as the maximum number of rejected exposures (defined as the percentage k_n of the number N_0 of requested exposures in section 6.3).

If $N_l \geq N_{lmin}$, the photometric properties of the equivalent long exposure can be computed. The average long exposure flux is:

$$F_l = \frac{1}{N_l} \sum_{j=1}^{N_l} F_d(j) \quad (42)$$

and the average background

$$Sbg_l = \frac{1}{N_l} \sum_{j=1}^{N_l} Sbg_d(j) \quad (43)$$

The rms flux variation computed during the long exposure:

$$F_{lrms} = \sqrt{\frac{1}{N_l} \sum_{j=1}^{N_l} (F_d(j) - F_l)^2} \quad (44)$$

The rms background variation

$$Sbg_{lrms} = \sqrt{\frac{1}{N_l} \sum_{j=1}^{N_l} (Sbg_d(j) - Sbg_l)^2} \quad (45)$$

Finally, the relative rms flux variation over the duration T_l , to be stored in the public database:

$$RF_{lrms} = \frac{F_{lrms}}{F_l} \quad (46)$$

The parameters characterizing the long exposure which are needed for further development are listed in Table 7.

Parameter	Variable	Unit
Number of Selected sequences	N_l	
Average Count	F_l	ADU
Average Background	Sbg_l	ADU
Rms Background Variation	Sbg_{lrms}	ADU
Shutter Open Time	T_s	s

Table 7: LOSSAM Long Exposure Parameters (internal history data)

7.3 Isoplanatic Angle

7.3.1 Theory

The isoplanatic angle θ_0 is defined as the angle from the axis of a wavefront sensor at which the variance of the phase excursion becomes superior to 1 radian squared⁶. It is expressed as:

$$\theta_0(\gamma, \lambda)^{-\frac{5}{3}} = 2.91(2\pi/\lambda)^2 \int_0^{z^{max}} C_n^2(z) z^{\frac{5}{3}} dz \quad (47)$$

where the integration is performed along the line of sight $z = h \cos(\gamma)$, γ is the zenith distance and h is the height above ground

This is to be compared to the expression of the scintillation index in the large aperture case, using the same variables, in the case of weak turbulence (Kolmogorov spectrum) and moderate airmass (smaller than 2):

$$S(\gamma, \lambda, D) = \int C_n^2(z) W(z, \lambda, D) dz \quad (48)$$

where $W(l, \lambda, D)$ is an aperture dependent altitude weighting function (from $\propto h^{\frac{5}{6}}$ for a point aperture to $\propto h^2$ for an infinite aperture). It has been shown⁷ that to a uniformly illuminated circular aperture of about 11 cm diameter (similar to the DIMM aperture size) corresponded a weighting function $\propto h^{\frac{5}{3}}$. This holds for weak turbulence around 10 km above ground which mostly contributes to scintillation:

$$W(z, \lambda, D) \approx A(\lambda, D) z^{\frac{5}{3}} \quad (49)$$

The weighting function has been calculated for the actual DIMM apertures. When the pupil diameters D_1 and D_2 are slightly different, the weighting functions can also be averaged as in Fig. 4. Moreover the altitude weighting function is weakly wavelength dependent: taking the 500 nm value of A leads to +2%, -5% error on θ_0 between 400 to 700 nm⁸.

Comparing Eq. 47 and 48, the zenith isoplanatic angle θ_0 is

$$\theta_0 = A \cos \gamma^{-\frac{8}{5}} S^{-\frac{3}{5}}(\gamma, D_1, D_2) \quad (50)$$

7.3.2 Scintillation binning

In the following two cases, the θ_0 computation shall be cancelled:

1. Scintillation data cannot be used when the line of sight extinction monitor (§7.2) has declared the sky non photometric, ie:

$$RF_{lrms} > RF_{lrms}^{max} \quad (51)$$

2. A misalignment of the DIMM aperture mask can introduce vignetting producing an imbalance in the scintillation through the twin apertures, the smaller scintillation value corresponding to

⁶ *Anisoplanatism in Adaptive Optics*; D.L. Fried, JOSA, Vol.72, 1982, 52-61

⁷ *Turbulence of the Upper Atmosphere and Anisoplanatism*; G.C. Loos and C.B. Hogge, Appl. Opt. Vol.18, No.15, 1979, 2654-2661

⁸ M.Sarazin, A.Tokovinin, *The Statistics of Isoplanatic Angle and Adaptive Optics Time Constant derived from DIMM data*; Beyond Conventional Adaptive Optics, ESO Conf. Proceedings, Venice, March 2001.

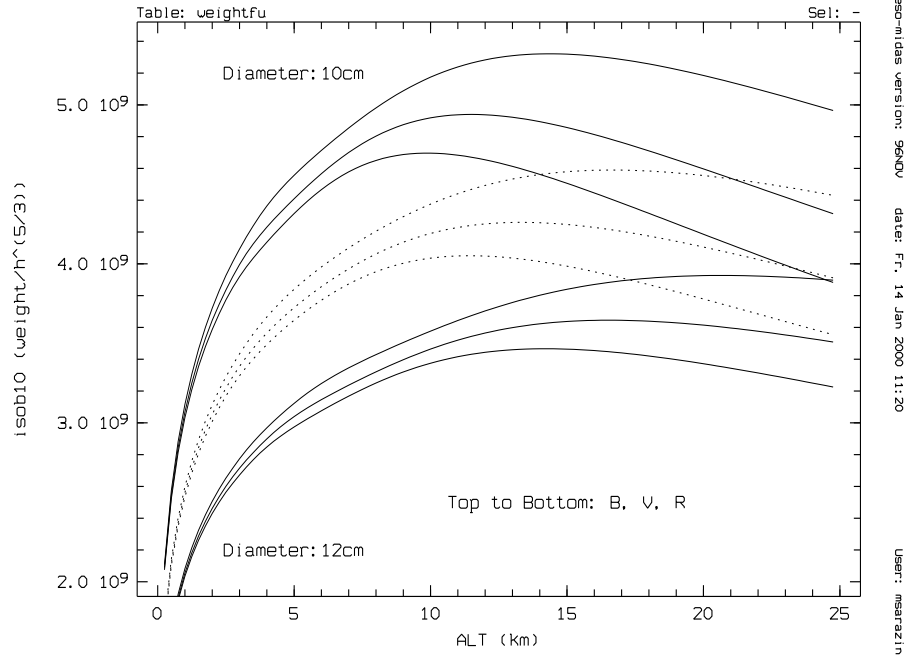


Figure 4: Altitude dependency of scintillation aperture weighting functions: the weighting functions divided by $h^{\frac{5}{3}}$ for 10 cm and 12 cm apertures (and the average of both) are shown for B, V and R observing wavelength. The rms variation of the V coefficient is less than 10% from 3 to 25 km, and less than 5% from 5 to 25 km. The value at 10 km altitude of average of the 10 and 12 cm V coefficients is 4.12 E+09

the least vignettted aperture. In such a case, the fluxes should also show a clear dissimilarity. The measurements shall be rejected if one if the relative differences verify the double inequality:

$$2|S_1 - S_2|/(S_1 + S_2) > DRS_{max}$$

AND

$$2|F_1 - F_2|/(F_1 + F_2) > DRF_{max}$$

The sequence average scintillation index in ‰ is:

$$S_d = \frac{1}{2}(S_1 + S_2) \quad (52)$$

The subsequent computation is similar to section 7.2.3, with S_l , the equivalent long exposure average scintillation index defined as

$$S_l = \frac{1}{N_l} \sum_{j=1}^{N_l} S_d(j) . \quad (53)$$

7.3.3 Exposure time correction

Because the scintillation is measured on images of finite exposure time T_d , the fast moving turbulence effects are averaged out. It has been shown (footnote 8) that the scintillation exposure time bias is a function of the wind velocity V_{200mb} measured at 200 mb (12 km above sea level).

The ECMWF wind velocity forecasts are available in 6-hour steps, updated normally twice a day at after 1UT and 6UT. An intranet access to acambi.hq.eso.org is possible from authorized machines, to retrieved the ASCII files:

`/diskb/asmpredi/Verif/site/200mb.ws` (*site* stands for *Paranal* or *LaSilla*, case sensitive)

A public access is possible at:

<http://www.eso.org/gen-fac/pubs/astclim/forecast/meteo/verification/site/images/200mb.ws>

The files contain 83 lines of data of the past 2 weeks and of the next 8 days, each line has the following format

FIELD 1 4 I4 :year

FIELD 6 7 I2 :month

FIELD 9 10 I2 :day

FIELD 16 17 I2 :hour

FIELD 24 28 f5.1 :local

FIELD 35 39 f5.1 :analysis

FIELD 46 50 f5.1 :forecast

FIELD 57 61 f5.1 :kalman

The column *forecast* contains the wind velocity V_{200mb} expressed in units of dm/s. A value of 999.0 means no data available. V_{200mb} is computed at the current time by linearly interpolating the two nearest forecast values, and converted in m/s.

The corresponding exposure time bias is extracted from the table *bias-5ms-11cm.inp* (available in ASCII format at <http://www.eso.org/gen-fac/pubs/astclim/forecast/meteo/CIRA/images/repository/teta0/bias-5ms-11cm.inp>), also by linear interpolation. The first column is the mean path P_S of the scintillating layers

$$P_S = 100T_d V_{200mb} ; \text{m}, \quad (54)$$

and the second column is the scintillation bias B_S ($B_S \in [0, 1]$, unitless) from which one can readily compute the scintillation coefficient at Zenith, corrected from exposure time:

$$S_0 = \frac{S_l}{B_S} \cos \gamma^{\frac{8}{5}} \quad (55)$$

7.3.4 θ_0 computation

The isoplanatic angle, θ_0 is then computed using equ. 50 with the value of A calculated at 500 nm for the diameter D of the DIMM apertures :

$$\theta_0 = 0.124 \cos \gamma^{-\frac{8}{5}} (S_l/B_S)^{-\frac{3}{5}} = 0.124 S_0^{-\frac{3}{5}} ; \text{arcsec}. \quad (56)$$

θ_0 is to be stored in the public database.

7.3.5 \bar{h} computation

The characteristic altitude of the turbulence, or mean turbulence height \bar{h} , is defined as:

$$\bar{h} = \left[\frac{\int dh h^{\frac{5}{3}} C_n^2(h)}{\int dh C_n^2(h)} \right]^{\frac{3}{5}} \quad (57)$$

Using Eq. 47 and 30, \bar{h} can thus be written as a function of zenith seeing and isoplanatic angle, expressed in arcsec along:

$$\bar{h} = \frac{6520}{\theta_0 \text{FWHM}_l} ; \text{m} \quad (58)$$

where the long exposure zenith seeing is computed as above along:

$$\text{FWHM}_l = \frac{1}{N_l} \sum_{j=1}^{N_l} \text{FWHM}_d(j) . \quad (59)$$

7.3.6 Data output

The parameters characterizing the isoplanatic angle are listed in Table 8.

Parameter	Variable	Unit
Long Exposure Scintillation	S_l	%
200mb Wind	V_{200mb}	m/s
Scintillation Bias	B_S	
Characteristic Altitude	\bar{h}	m

Table 8: Teta0 Parameters (internal history data)

7.4 Coherence Time

7.4.1 Direct Measurement

A direct measurement of τ_0 requires fixed time intervals of 1-2 ms between several successive exposures of 1-2 ms duration. Using the VLT-TCCD installed in the ASM, this is possible only by vertically shifting a few lines of the CCD into the storage area after each exposure, and read-out the image when full. The image processing is then similar to the seeing monitor mode, with several twin images per frame. An additional N-elements time series of dX/dt and dY/dt differential velocities is obtained. The time dt between exposures has to be reproduced with an accuracy better than 10%. This option is not yet implemented but the existing hardware is compliant.

7.4.2 τ_0 computation from ASM and meteorological data

It has been shown empirically⁹ that the average velocity V^* of the wavefront over chilean sites is related to the velocity at the 30 m level V_{30m} and at the 200 mb level V_{200mb} by:

$$V^* = \text{MAX}(V_{30m}, 0.4V_{200mb}) . \quad (60)$$

The wind velocity at 30 m above ground, V_{30m} , is available from the meteorological station (1 mn average Vaisala parameter **WS1S**). The wind velocity at 200 mb, V_{200mb} , has been retrieved in section 7.3.3.

The coherence time for adaptive optics τ_0 is defined as¹⁰

$$\tau_0 = 0.31 \frac{r_0}{V^*} . \quad (61)$$

Using the definition of r_0 in equ. 30, the coherence time is expressed as a function of the seeing along:

$$\tau_0 = 0.31 \frac{0.976\lambda}{\rho} \frac{1}{\text{FWHM}} \frac{1}{V^*} , \quad (62)$$

where λ is the reference wavelength and ρ is the arcsec to radian conversion factor, both given in Table 3.

τ_0 is to be stored in the public database as the 1 mn average coherence time, in seconds. The parameters characterizing the coherence time are listed in Table 9.

Parameter	Variable	Unit
Average wavefront velocity	V^*	m/s
Wind velocity at 30 m	V_{30m}	m/s

Table 9: Tau0 Parameters (internal history data)

⁹M.Sarazin, A.Tokovinin, *The Statistics of Isoplanatic Angle and Adaptive Optics Time Constant derived from DIMM data*; Beyond Conventional Adaptive Optics, ESO Conf. Proceedings, Venice, March 2001.

¹⁰F. Roddier, J.M. Gilli and G. Lund; *On the origin of speckle boiling and its effects in stellar speckle interferometry*, J. Optics, 1982, **13**, 5, 263-271.

8 Summary of airmass and wavelength dependency for asm parameters

All asm parameters are delivered for zenith observation at 0.5μ wavelength. It may be however of interest for comparison purposes to convert them to the science observation airmass (AM) and wavelength (λ in μ). The following set of equations should be used:

$$\text{FWHM}(\text{AM}, \lambda) = \text{FWHM} \left(\frac{0.5}{\lambda} \right)^{1/5} \text{AM}^{3/5} \quad (63)$$

$$r_0(\text{AM}, \lambda) = 0.976 \frac{\lambda}{\text{FWHM}(\text{AM}, \lambda)} = r_0 \left(\frac{0.5}{\lambda} \right)^{-6/5} \text{AM}^{-3/5} \quad (64)$$

$$\tau_0(\text{AM}, \lambda) = \tau_0 \left(\frac{0.5}{\lambda} \right)^{-6/5} \text{AM}^{-3/5} \quad (65)$$

$$\theta_0(\text{AM}, \lambda) = \theta_0 \left(\frac{0.5}{\lambda} \right)^{-6/5} \text{AM}^{-8/5} \quad (66)$$